AIAA SciTech Forum
9 - 13 January 2017, Grapevine, Texas
55th AIAA Aerospace Sciences Meeting

10.2514/6.2017-0661

Quantal treatment of O_2–Ar vibrational relaxation at hypersonic temperatures

Inga S. Ulusoy * Daniil A. Andrienko† Iain D. Boyd ‡ Rigoberto Hernandez §

An investigation of rotational and vibrational relaxation in O_2–Ar collisions is carried out using the multi-configuration time-dependent Hartree and quasiclassical trajectory methods. The vibrational relaxation times are compared with the new highly accurate experimental data provided by the experimental group in Stanford University in the range of temperatures between 1000 and 7,000 K. Atom-diatom collisions are simulated as the first step in developing the aerothermodynamics models based on first principles. The relaxation times obtained via quantum approach demonstrate very good agreement the experimental measurements conducted in shock tube facilities. At the same time, the quasiclassical simulation fails to predict rates of vibrationally inelastic transitions at temperatures lower than 3000 K. This observation and the computational cost of adopted methods suggest that the next generation of thermochemical models should be a combination of quantum and quasi-classical approaches.

Nomenclature

v, j	pre-collisional vibrational and rotational quantum numbers
v', j'	post-collisional vibrational and rotational quantum numbers
k	rate coefficient of bound-bound transition, cm^3/s
J	total angular momentum of O_2–Ar system
T, T_r, T_v	translational, rotational and vibrational temperatures, K

I. Introduction

Vibrational and rotational energy transfer in atom-molecule collisions is triggered by the high temperature environment during a flight of a hypersonic vehicle. The shock heated flow around a vehicle disrupts the equilibrium population of states in ambient air, thereby inducing a nonequilibrium distribution [1, 2]. The reorganization of molecular states and the return to a new equilibrium distribution requires a characteristic amount of time. Energy is exchanged in molecular collisions between the translational, rotational and vibrational modes of collision partners. The readjustment of translation and rotational modes typically happens much faster than the readjustment of the vibrational modes or chemical reactions. Thus, at moderate hypersonic speeds, i.e. less than 3 km/s, the main processes governing the energy dissipation are vibrational energy transfer and dissociation [3–5].

An understanding of vibrational relaxation is therefore crucial for realistically modeling hypersonic air flows. Vibrational relaxation of molecular species is governed by two processes, the vibration-vibration (VV) energy transfer and the vibration-translation (VT) energy transfer. In the former process, vibrational energy from one diatomic is transferred to another diatomic, effectively exciting and de-exciting vibrational levels of the collision partners. The net energy exchange between vibrational degrees of freedom (DOF)

*Research Associate, Department of Chemistry, Michigan State University, 578 S Shaw Lane, East Lansing, MI 48824
†Postdoctoral research fellow, Department of Aerospace Engineering, University of Michigan, 1320 Beal Ave, Ann Arbor, Michigan 48109
‡James E. Knott Professor, Department of Aerospace Engineering, University of Michigan, 1320 Beal Ave, Ann Arbor, Michigan 48109
§Professor, Department of Chemistry, Johns Hopkins University, 138 Remsen Hall, 3400 N. Charles Street, Baltimore, MD 21218

strongly correlates with vibrational anharmonicity. Such energy exchange takes place rapidly and with a high probability at low translational temperatures and in cooling flows with high internal temperature [6]. On the other hand, the vibration-to-translation (VT) energy transfer is a dominant mechanism of relaxation at high temperature conditions. In the VT energy transfer, the energy corresponding to a vibrational (de-)excitation is exchanged with the translational degrees of freedom.

The processes investigated here take place in the upper atmosphere, where the gases N_2 and O_2 are the most predominant compounds. Here, we choose to investigate the O_2–Ar system for its simplicity and availability of experimental data on vibrational relaxation [7, 8]. Once the methodology is established, the routine can be applied to more complex systems such as O_2–O, O_2–O_2, etc. We use the quantum dynamics multi-configuration time-dependent Hartree method (MCTDH) [9–11] and a quasi-classical trajectory (QCT) method to derive the rate coefficients for vibrational transitions in O_2–Ar scattering in a wide range of translational temperatures:

$$O_2(v) + \mathrm{Ar} \rightarrow O_2(v') + \mathrm{Ar} \tag{1}$$

During this vibrationally inelastic collision, an energy exchange between the vibrational DOF of the diatomic molecule and the translational DOFs of the atom takes place. This process of energy transfer is characterized by its rate coefficient, and we can derive rate coefficients for the excitation as well as the de-excitation collisions. These rates are connected to the vibrational relaxation time, and to the energy-equivalent vibrational temperature of the gas. Under nonequilibrium conditions the vibrational, translational and rotational temperatures in gas flows around hypersonic vehicles are not equal, and the distribution of states can deviate from a Boltzmann distribution. Therefore, nonequilibrium effects in the relaxation dynamics need to be taken into account. The present work is a first step in this direction, since the transition probabilities calculated here can be used in any nonequilibrium distribution to derive the rate coefficients. Any desired distribution of states can be input into our code for the rate calculation, yielding a nonequilibrium rate in a manner of seconds. The generated rates can then be used in the computational fluid dynamics to aid the development of thermal protection systems and flow control strategies.

The quasi-classical methods are typically adopted for calculation of state-specific VT rates due to the significantly higher cost of more detailed quantum models [3, 5, 12, 13]. Here, we present a fully quantum dynamical approach for obtaining VT rates using a corresponding summation over the quantum states. At low temperatures, the QCT method fails to predict the VT rates accurately for molecular systems with strong repulsive potentials. This is due to the lack of detailed tunneling events and interference effects that occur with sufficient probability near threshold that the classical trajectories necessarily miss.

Using quantum simulations, we are able to bridge this gap and are able to estimate the relative accuracy of quantum and QCT rates. These rates can be converted into vibrational relaxation times, using derivations commonly applied in gas dynamics, [1] and thus can be compared to experimental data. In the temperature range discussed here (1000 K to 10,000 K), we obtain very good agreement between calculated and measured vibrational relaxation times. The important effects of vibrational energy relaxation (VER) between the colliding oxygens resolved earlier [14, 15] at low temperatures do not arise here because our mixtures consist of dilute O_2 which necessarily suppresses VER.

In the following, we discuss the theoretical basis for our quantum dynamics and QCT simulations in Sections A and B. Comparison of the analytical potential energy surface (PES) with the ab-initio PES calculations is provided as well. The standard model relating vibrational relaxation times to rate coefficients is discussed in Section C. We present transition probabilities, scattering cross sections, rate coefficients and vibrational relaxation times in Section III. Our findings are discussed in Section IV.

II. Theory

The physical basis of any dynamics calculation is the representation of the forces and their gradients. A PES with a pairwise combination of the Hulburt-Hirschfelder analytic function [16] with fitted parameters for the O_2 potential energy curve [17, 18] and the Buckingham potential [19] for the O–Ar interaction is used [20]. This methodology of constructing the many-body potential energy surface is widely adopted for extensive quasi-classical studies of diatom and inert atom collisions. [21, 22] The validity of this approach is based on the electronic structure of Ar ground electronic state, which has a closed-shell configuration [23]. The parameter values are given in Table 1.

$$V\left(r_{\mathrm{O}_a,\mathrm{O}_b}, r_{\mathrm{O}_a,\mathrm{Ar}}, r_{\mathrm{O}_b,\mathrm{Ar}}\right) = V_{\mathrm{O}_2}\left(r_{\mathrm{O}_a,\mathrm{O}_b}\right) + \sum_{i=a,b} V_{\mathrm{O}_i,\mathrm{Ar}}\left(r_{\mathrm{O}_i,\mathrm{Ar}}\right) \tag{2a}$$

$$V_{\mathrm{O}_2}\left(r_{\mathrm{O}_a,\mathrm{O}_b}\right) = D\left[\left(1-\exp^{-a\left(r_{\mathrm{O}_a,\mathrm{O}_b}-r_e\right)}\right)^2 + ca^3\left(r_{\mathrm{O}_a,\mathrm{O}_b}-r_e\right)^3 \exp^{-2a\left(r_{\mathrm{O}_a,\mathrm{O}_b}-r_e\right)}\left(1+ab\left(r_{\mathrm{O}_a,\mathrm{O}_b}-r_e\right)\right)\right] \tag{2b}$$

$$V_{\mathrm{O}_i,\mathrm{Ar}}\left(r_{\mathrm{O}_i,\mathrm{Ar}}\right) = A\exp^{-Br_{\mathrm{O}_i,\mathrm{Ar}}} - C\exp^{-\left(\frac{1.28r_{\mathrm{m}}}{\left(r_{\mathrm{O}_i,\mathrm{Ar}}-1.0\right)}\right)^2} / r^6_{\mathrm{O}_i,\mathrm{Ar}} \tag{2c}$$

$V_{\mathrm{O}_2}(r_{\mathrm{O}_a,\mathrm{O}_b})$			$V_{\mathrm{O}_i,\mathrm{Ar}}(r_{\mathrm{O}_i,\mathrm{Ar}})$		
parameter	value	unit	parameter	value	unit
a	2.653645	Å^{-1}	A	209.9357	E_h
b	1.670039		B	2.01690	a_0^{-1}
c	6.141914×10^{-2}		C	43.85140	$E_h a_0^6$
D	4.206738×10^4	cm^{-1}	r_{m}	6.42700	a_0
r_e	1.207520	Å			

Table 1: Potential parameters used in the dynamics study. Parameters for the O_2-potential are taken from Ref. [17,18]. Parameters for the O_i–Ar potential are taken from Ref. [20].

The zero-point energy for the O_2–Ar system using this PES is 788 cm^{-1} [exp. E_{ZPE}=787.4 cm^{-1} (Ref. [24])], and the first vibrationally excited level lies at E_{v_1}=1556 cm^{-1} [exp. E_{v_1}=1580 cm^{-1} (Ref. [25])], as calculated using the MCTDH method. [26]

The accuracy of the dynamics calculations depends on the accuracy of the PES employed in the dynamical simulation. To validate the accuracy of the (parameterized) model PES in Eq. 2 with respect to the O_2-Ar interaction, we performed CCSD/6-311(d,p) calculations using the GAMESS-US program package. [27–29] Triplets led to negligible corrections and were excluded.

CCSD calculations are performed for several O–O bond lengths. Namely, the equilibrium point (EQ) 1.207 Å, the left turning (LT) point and the right turning (RT) point of the O_2 state with v=0, j=0 are chosen as well. The LT point correspond to the O–O distance of 1.159 Å, the RT point is located at 1.263 Å. Additionally, CCSD calculations have been performed at left turning point (LT2) of state v=1, j=218 at 1.359 Å and at the distance of 1.7 Å (RT2) which is close to the location of the right turning point for the rovibrational state ($v = 1, j = 218$). All CCSD calculations are performed at different angles between O–O internuclear axis and the line between Ar and O_2 center of mass. Specifically, calculations reflect the potential at 0, 5, 10, 20, 40, 60, 80 and 90 degrees of collisions. This angle is referred to as the impact angle in future discussions.

The comparison of the CCSD and analytical potentials is given in Figs. 1a - 3a. For left turning points (LT and LT2) and for the equilibrium distance (EQ) the analytical potential generally overestimates the CCSD data. This overestimation is quite significant: at small, but yet classically accessible distance between Ar and O_2 center of mass, the CCSD potential is smaller than the analytical potential by 1 eV.

On the other hand, the behavior of the CCSD potential at RT and RT2 distances raises some questions. The O_2 electronic structure is quite complicated, due to many different spin states lying close in energy as the O_2 is dissociating. This becomes obvious from the CCSD calculations. While obtaining potential energy curves for O_2 bond lengths close to the equilibrium is straightforward, for longer O_2 bond length the other spin states lie closer in energy and become accessible. For these geometries, the CCSD calculations do not converge at all, or they converge to a wrong electronic state. This is reflected in the discrepancies of the curves for 20 and 80/90 degrees for O_2 right turning point in Fig. 2b. While all energies obtained are for a triplet electronic state, the higher-lying points at closer O–Ar distance for 80 and 90 degrees reflect a high spin density on the Ar atom instead of only on the O_2 atoms. The situation becomes worse for larger O_2 bond lengths. The difficulty in reproducing the electronic structure of dissociating O_2 is well known [30,31]. To obtain the electronic structure correctly, the multi-reference character of the electronic wave function must be explicitly considered in the electronic structure calculations.

At moderate distances between O_2 and Ar the CCSD calculations indicate the existence of a well before the potential turns into a repulsive wall. The close-up of the CCSD potential at the LT2 distance is shown in Fig. 3b. The depth of potential well increases with the impact angle. The minimum of the CCSD potential is reached at 80 ° and is equal to 0.008 eV. This value is much smaller than size of O_2 vibrational quanta, thus it should be relatively unimportant for vibrational relaxation. At the same time, the depth of well is approximately 45 times larger than O_2 rotational constant and, thus, it may be important for rotational relaxation of cold molecules. The present depth of potential well can be implemented in analytical theories such as the FHO or SSH models [32] in order to obtain more accurate transition rates.

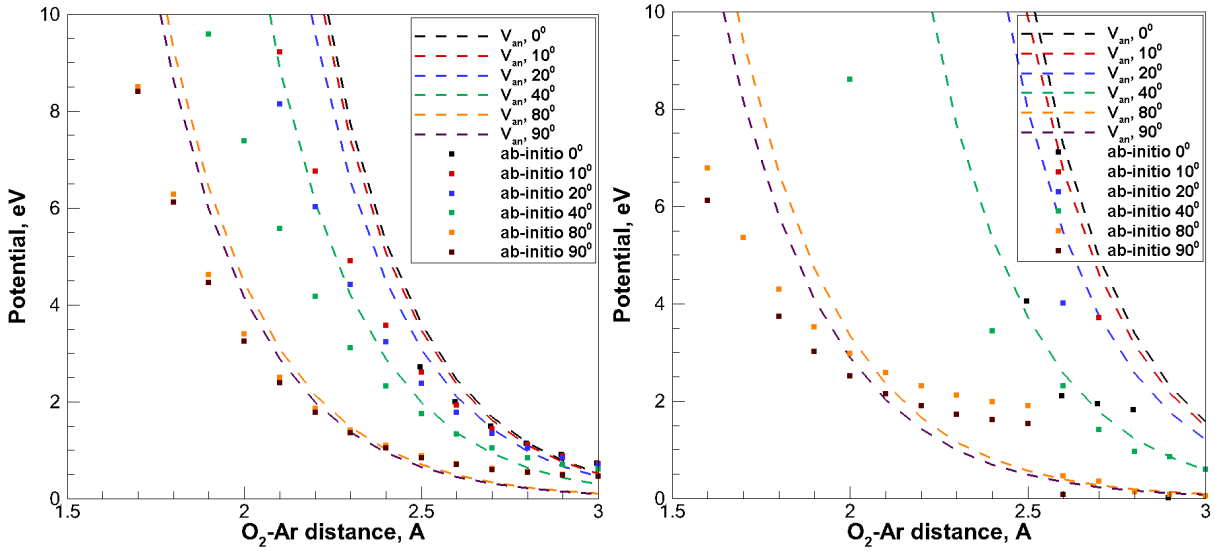

(a) O_2 LT2 distance (b) O_2 RT2 distance

Fig. 1: CCSD and analytical potentials at LT2 and RT2 O–O bond length

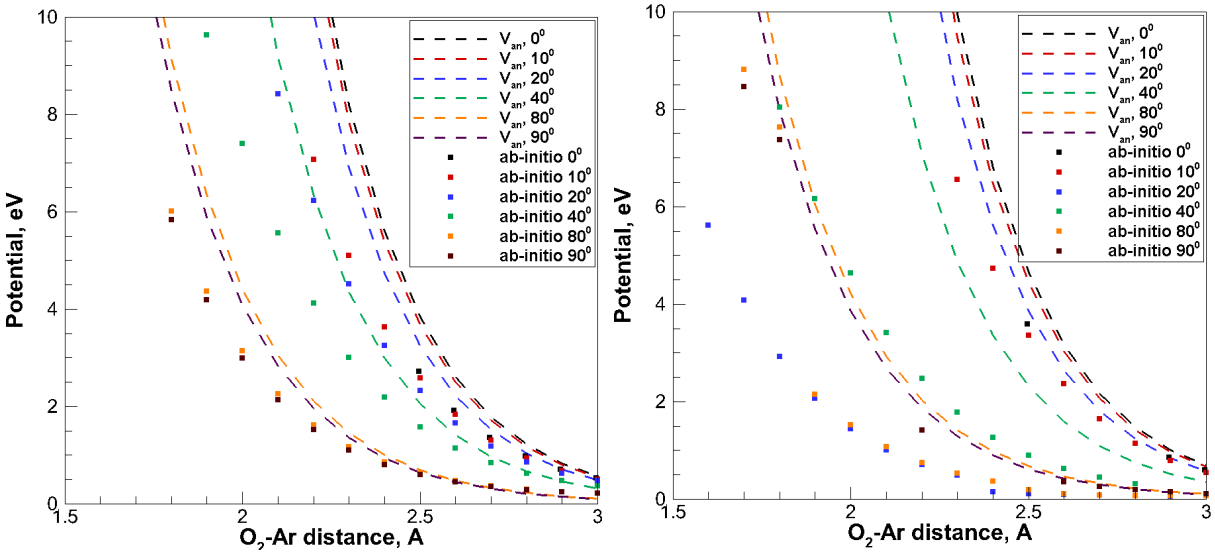

(a) O_2 LT distance (b) O_2 RT distance

Fig. 2: CCSD and analytical potentials at LT and RT O–O bond length

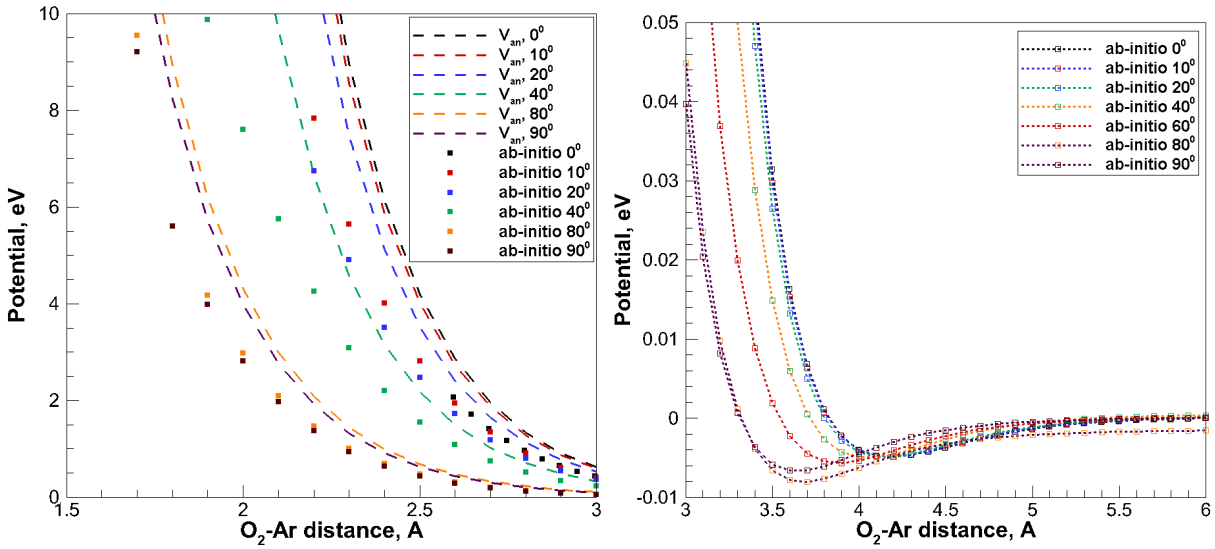

(a) CCSD and analytical potentials at O_2 EQ distance

(b) Close-up of CCSD potential at LT2 distance

Fig. 3: CCSD and analytical potentials at EQ and LT2 O–O bond length

A. Quantum Dynamics

The implementation of the MCTDH method [9] by the group of H.-D. Meyer [26] is used in the present work to compute the quantum-mechanical rates and cross sections. Here, the nuclear wave function is approximated as a product of single-particle functions (SPFs)

$$\Psi(Q_1,\ldots,Q_f,t)=\sum_{j_1=1}^{n_1}\cdots\sum_{j_f=1}^{n_f}A_{j_1\ldots j_f}(t)\prod_{\kappa=1}^{f}\phi_{j_\kappa}^{(\kappa)}(Q_\kappa,t) \tag{3}$$

for f DOFs, and n SPFs per DOF. The SPFs are represented as a linear combinations of the primitive grid basis. The equations of motion (EOM) for the SPFs and the time-dependent coefficients $A_{j_1\ldots j_f}(t)$ involve the computation of the mean fields $\langle H_R\rangle_{jl}^{\kappa}$ at each time step, which is the most computationally demanding step in the propagation. By rewriting the Hamiltonian such that h_κ operates only on the κ degree of freedom, and approximating the residual Hamiltonian H_R as a sum of products of single-particle operators,

$$H=\sum_{\kappa=1}^{f}h_\kappa+H_R \tag{4}$$

$$H_R=\sum_{r=1}^{s}c_r\prod_{\kappa=1}^{f}h_r^{(\kappa)} \tag{5}$$

the multi-dimensional integrals required in the evaluation of the mean fields are circumvented. The kinetic operator is usually separable between the DOF, but the potential term must be fitted to this form [33] . We achieve a product representation of the potential by fitting it using the potfit program, as part of the MCTDH package. To reduce the grid size required in the computation, and to compute the reactive and inelastic fluxes, complex absorbing potentials (CAPs) are added to the Hamiltonian for each DOF [34, 35]. These CAPs have the form of

$$-iW(Q)=-i\eta(Q-Q_c)^b\theta(Q-Q_c) \tag{6}$$

where in our calculations, the order of the CAPs is three ($b=3$), and the grid point Q_c denotes the position at which the CAP is switched on, with $\theta(Q-Q_c)$ the Heaviside step function. The parameter η denotes the CAP strength.

The reactant Jacobi coordinates comprise our choice for the coordinate system and consist of the vibrational coordinate r_2 (O-O distance), translational coordinate r_1 (distance of Ar to the center of mass of the O_2 molecule), and the angle θ between r_1 and r_2. In this coordinate system, the center of mass is constant. We can define the quantum numbers as v for vibrational quanta, j for rotation of the diatomic, J for the total angular momentum quantum number, and K for the projection onto the body-fixed axis. The Hamiltonian of the scattering system is defined in the coupled-states (CS) approximation, where J and K are "good" quantum numbers (neglecting J,K-coupling):

$$\hat{H} = -\frac{1}{2\mu_{r_1}}\frac{\partial^2}{\partial r_1^2} - \frac{1}{2\mu_{r_2}}\frac{\partial^2}{\partial r_2^2} + \frac{\hat{\jmath}^2}{2\mu_{r_2} r_2^2} + \frac{j(j+1)}{2\mu_{r_2} r_2^2} + \frac{1}{2\mu_{r_1} r_1^2}\left(J(J+1) - 2K^2 + \hat{\jmath}^2\right) + V(r_1, r_2, \theta) \tag{7}$$

$$\hat{\jmath} = -\left(\frac{1}{\sin\theta}\frac{\partial}{\partial\theta}\sin\theta\frac{\partial}{\partial\theta} - \frac{K^2}{\sin^2\theta}\right) \tag{8}$$

The reduced masses μ_{r_1} and μ_{r_2} are the reduced masses of the O_2–Ar and O_2-system, respectively. The PES $V(r_1, r_2, \theta)$ is specified in the previous section. To obtain scattering cross sections and rate constants, inelastic transition probabilities need to be calculated. In principle, the inelastic transition probabilities can be obtained by two different methods. For state-specific transition probabilities $P_{if}(E)$ the method developed by Tannor and Weeks [36] is most suitable, where the S-matrix elements are obtained from the cross-correlation function $C_{if}(t)$. Final-state averaged transition probabilities can then be obtained by summation over the final states f

$$P_i(E) = \sum_f P_{if}(E) \tag{9}$$

A more direct way to obtain the final-state averaged transition probabilities is by evaluating the flux through the CAP W (see Eq. (6)). This directly yields $P_i(E)$ as

$$P_i(E) = \frac{2}{\pi|\Delta(E)|^2}\mathrm{Re}\int_0^\infty g(\tau)e^{-iE\tau}d\tau \tag{10}$$

$$g(\tau) = \int_0^\infty dt\,\langle\Psi(t+\tau)\,|W|\,\Psi(t)\rangle \tag{11}$$

The energy distribution of the initial and final wave packets, $\Delta_i(E)$ and $\Delta_f(E)$, are obtained by diabatic correction of the translational DOF, where the influence of the interaction potential along r_1 is corrected for. The energy distribution is evaluated as the overlap of the translational SPF with a distorted wave (rather than a plane wave for a Gaussian initial SPF):

$$\Delta(E) = \langle\Psi_{\mathrm{dist}}|\Psi_0\rangle = \sqrt{\frac{\mu_{r_1}}{2\pi}}\int_0^\infty \frac{\exp\left(i\int_{r_1}k(x)dx\right)}{k(r_1)}\chi_0(r_1)dr_1 \tag{12}$$

where the distorted wave Ψ_{dist} is represented by a WKB-wave (Wentzel-Kramer-Brillouin) multiplied with the r_2 eigenstate SPF. The associated local momentum $k(r_1)$ is defined as the momentum available for r_1

$$k(r_1) = \sqrt{2\mu_{r_1}(E - \bar{V}_v(r_1))} \tag{13}$$

with $\bar{V}_v(r_1)$ the diabatic mean-field potential. In contrast to the initial wave packet, its energy distribution depends on the internal state of the scattering system (vibrational state v, rotational state j, total rotational angular momentum J and its projection K onto the body-fixed axis). Since for the scattering cross section, the transition probability needs to be expressed in terms of the collision energy E_{col} (purely translational energy), the energy shift due to the internal state of the molecule is corrected for.

The flux can be projected onto final vibrational states v' by applying a projection operator to the wave packets in Eq. (11). In this way, the required transition probabilities from initial to final vibrational state, $P^{JK}_{vj\to v'}$, can be obtained. Since we are interested in highly averaged properties such as cross sections and rate

constants, we calculate only final-state averaged transition probabilities which already implicitly contain the summation over final rotational states j', J', and K'.

The integral cross sections $\sigma_{vj\to v'}(E_{\rm col})$ are then obtained as [37]

$$\sigma_{vj\to v'}(E_{\rm col}) = \frac{\pi\hbar^2}{2\mu_{r1}E_{\rm col}} \sum_{J=0}^{J_{\rm max}} \sum_{K=-\min(J,j)}^{K=\min(J,j)} \frac{(2J+1)}{(2j+1)} P^{JK}_{vj\to v'}(E_{\rm col}) \tag{14}$$

The integral cross sections are required over an energy range of 5.0 eV. Within this energy range, there is a large amount of internal states that need to be included. In order to reduce the computational effort, we assume that the dependence of $P^{JK}_{vj\to v'}$ on J can be obtained by an energy shift as for example in the J-shifting approximation, [38] or the quantum analog of the capture model: [39]

$$P^{JK}_{vj\to v'}(E) = P^{0,K}_{vj\to v'}(E - E_{\rm shift}) \tag{15}$$

$$E_{\rm shift}(r_1) = \langle vj|V|vj\rangle + \frac{\hbar^2}{2\mu_{r1}r^2_{1,\rm barr}} J(J+1) \tag{16}$$

Here, the shifting energy is the barrier associated with an effective potential. The distance $r_{1,\rm barr}$ is associated with the distance of the rotational barrier, and can be related to the QCT parameter $b_{\rm max}$. The K-dependence of $P^{JK}_{vj\to v'}$ is assumed to be negligible, so that

$$P^{JK}_{vj\to v'}(E_{col}) = P^{J,0}_{vj\to v'}(E_{col}) \tag{17}$$

The integral cross sections are then rotationally averaged over the initial rotational states of the diatomic

$$\sigma_{v\to v',T}(E_{\rm col}) = \sum_{j=1}^{j_{\rm max}} p(j,T)\sigma_{vj\to v'}(E_{\rm col}) \tag{18}$$

$$p(j,T) = \frac{(2j+1)\exp^{-\beta E_{rot}}}{Q_{\rm rot}(T)} \tag{19}$$

$$Q_{\rm rot}(T) = \sum_{j=1}^{j_{\rm max}} (2j+1)\exp^{-\beta E_{rot}} \tag{20}$$

Here, $\beta = (k_{\rm B}T)^{-1}$ with $k_{\rm B}$ the Boltzmann constant. Due to the O_2 nuclear spin state, only odd rotational states can be populated. Consequently the even states can be ignored in the sum. Translational averaging of the cross sections yields the vibration-translation transition rate coefficients

$$k_{v\to v'}(T) = g_s \int_0^{E_{\rm max}} \sqrt{\frac{8}{\pi\mu_{r1}}}\beta^3 e^{-\beta E_{\rm col}} \cdot \sigma_{v\to v',T}(E_{\rm col}) E_{\rm col} dE_{\rm col} \tag{21}$$

with $g_s = 1/3$ the factor of spin degeneracy, and k in units of $\rm cm^3/s$. The value of g_s comes from the ratio of the degeneracies of PES and reactants [21]. Below, we calculate vibrational transition rates from vibrational level $v = 1$ to all vibrational levels $v = x, \{x = 0, 2, 3, \ldots, 36\}$, thus obtaining rates of vibrational deactivation, $k_{v\to v'}(v > v')$, as well as rates of vibrational activation, $\rm k_{v'\to v}$. The rates of vibrational activation can be transformed into rates of vibrational deactivation using the principle of detailed balance, assuming the system is in an equilibrium state:

$$k_{v'\to v} = k_{v\to v'} \cdot \exp^{-\beta E_{vib}}, \tag{22}$$

where E_{vib} is the difference in vibrational energy between the v and v' states.

For another point of comparison with experimental and empirical data, we also compute temperature-dependent transition probabilities. First, the final-state averaged transition probabilities are averaged over J:

$$P_{vj\to v'}(E_{\rm col}) = \frac{\sum_J^{J_{\rm max}}(2J+1)(2\min(j,J)+1)P^J_{vj\to v'}(E_{\rm col})}{\sum_J^{J_{\rm max}}(2J+1)(2\min(j,J)+1)} \tag{23}$$

These probabilities are then averaged over rotational states, and integrated over the energy range $E_{\rm col}$ while normalizing the integral

$$P_{v\to v',T}(E_{\rm col}) = \sum_{j=1}^{j_{\max}} p(j,T) P_{vj\to v'}(E_{\rm col}) \tag{24}$$

$$P_{v\to v'}(T) = g_s \int_0^{E_{\max}} \sqrt{\frac{8}{\pi\mu_{r1}}\beta^3} e^{-\beta E_{\rm col}} \cdot P_{v\to v',T}(E_{\rm col}) E_{\rm col} dE_{\rm col}/N \tag{25}$$

$$N = \int_0^{E_{\max}} \sqrt{\frac{8}{\pi\mu_{r1}}\beta^3} e^{-\beta E_{\rm col}} E_{\rm col} dE_{\rm col} \tag{26}$$

B. Quasi-classical trajectory calculations

The QCT method is used to reduce the computational cost of generating the O_2–Ar vibrationally-resolved cross sections. Details of this approach are given elsewhere [40]. Here, we briefly discuss the basics of this method. The initial rovibrational state of the oxygen molecule, (v, j), is fixed in each batch of trajectories. The internuclear separation of the isolated oxygen molecule is initialized by the random sampling of vibrational phase based on the period of motion. The initial separation of the target and projectile particles is given by 15 Å. Hamilton's differential equations are solved by the Adams-Moulton method to $11^{\rm th}$ order of accuracy as described in Ref. [40]. The impact parameter, b, is sampled with a step size of 0.1 Å. Every batch contains 2×10^3 trajectories. Analysis of the final state is performed according to Ref. [40]. Each trajectory is integrated with an error in the total energy not exceeding $10^{-4}\%$. A trajectory is terminated after the distance between products exceeds the initial separation. Each such trajectory is then classified into one of three possible channels: inelastic non-reactive (as in a bound-bound transition with the change of O_2 initial rovibrational state), elastic non-reactive (with no change of O_2 initial rovibrational state) and dissociation (bound-free transition). The probability of the state-specific transition $(v, j) \to (v', j')$ at a given collision energy E_{col} is defined as follows:

$$P_{vj\to v'j'}\left(E_{col}\right) = \frac{2}{b_{max}^2}\int_0^{b_{max}} \left(\frac{N_{(vj)\to(v'j')}}{N}\right) bdb, \tag{27}$$

where b_{max} is the impact parameter at which only elastic collisions are observed, $N_{(vj)\to(v'j')}$ and N are the number of trajectories with the desired transition and the total number of trajectories in the current batch of impact parameter, respectively. The cross section of a bound-bound transition is calculated as follows:

$$\sigma\left(E_{col}, v, j\right) = \pi b_{max}^2 P\left(E_{col}, v, j\right), \tag{28}$$

where P is sampled over the five variables, not explicitly mentioned in its argument in Eq. (28): the impact parameter b, the initial azimuthal and polar orientations of the target molecule, the initial orientation of the target molecule angular momentum and the initial vibrational phase of the target molecule. The present QCT calculations study dynamics of O_2–Ar collisions in the range of collision energy from 0.1 to 5 eV. This range is covered by 35 intervals of uneven length. Stratified sampling of the impact parameter is adopted to increase accuracy of statistical modeling. The present study features the analysis of rates assuming trans-rotational equilibrium. In order to do so, the cross section of transition from the initial rovibrational state to any final rotational state of the final vibrational level is computed using Eq. (20). The corresponding rate of transition is obtained using Eq. (21).

C. Vibrational relaxation time

The rate coefficients for vibrational deactivation can be related to vibrational relaxation time as derived from experimental data by Millikan and White, [41] Camac [7] and recent measurements by Owen and co-workers [8]. The vibrational relaxation parameter τ, is expressed in Landau-Teller theory as [1]

$$p\tau_{vib}(T) = \frac{1}{\beta k_{v=1\to v'=0}(T)\cdot\left(1-e^{-\beta E_{\rm vib}}\right)} \tag{29}$$

with $\beta = 1/kT$, pressure p, and energy difference E_{vib} of the vibrational states v' and v. In this approach, the de-excitation from the first excited state ($v = 1$) to the ground vibrational state ($v' = 0$) is considered.

The exponential term in Eq. (29) corresponds to the contribution of the reverse excitation process. When the excitation of vibrational ground state is improbable (i.e. $E_{vib} \gg 1/\beta$), Eq. (29) simplifies to:

$$p\tau_{vib}(T) = \frac{1}{\beta k_{v=1\rightarrow v'=0}(T)}. \tag{30}$$

Equation (30) is based on the assumption that the population of vibrational level $v = 1$ is very small compared to the vibrational ground state. However, at temperatures relevant to hypersonic flows, the resulting population of excited vibrational states and the contribution of multiquantum transitions lead to relaxation times that are significantly different from those obtained assuming a two-state vibrational model. Given the complete set of relevant transitions for each internal state, one can then define the average relaxation time for the entire rovibrational ensemble. This was previously done for N_2–N (Ref. [42]) and O_2–O (Ref. [43]) molecular systems using the database of rates generated by the QCT method. The details of such simulations, involving the master equation solution, are given elsewhere. [43] In the present work, the O_2–Ar vibrational relaxation time is obtained using the e-folding method [44] from the O_2–Ar set of vibrationally-resolved transitions rates assuming rotational equilibrium. Unfortunately, due to the high cost of the fully quantum approach, such simulations using the MCTDH method are currently computationally intractable.

In experiments, the vibrational relaxation time is obtained as the slope of the straight line fit to the measured profile of $\log(1 - E/E_f)$ over laboratory time t, with E the energy in the vibrational state, and E_f the final vibrational energy. This involves a number of approximations, such as vibrational harmonicity and single-state quantum transitions, as in Landau-Teller theory. An empirical model of the relation between vibrational relaxation time and temperature is detailed in Millikan and White [41] for various scattering systems. The same dependence is observed for a large number of species with a strong repulsion between projectile and target particles. Below, we compare calculated vibrational relaxation times (for the above equations) with experimental ones, and with vibrational relaxation times obtained using master equation calculations based on computed rates.

D. MCTDH computational details

For all quantum propagations, we use the constant-mean field (CMF) integration scheme, with a Bulirsch-Stoer (BS) extrapolation scheme for the propagation of SPFs and a short iterative Lanczos (SIL) algorithm for the A-vector propagation. This is implemented in the MCTDH package version release 84.8 [45]. The DVR grids used to represent the primitive basis run from $r_1^{\min} = 3.89\,a_0$ to $r_1^{\max} = 10.0\,a_0$, and $r_2^{\min} = 1.78\,a_0$ to $r_2^{\max} = 6.00\,a_0$, where a Sine DVR is used for both DOFs, and the number of grid points is $n_{r_1} = 512$ and $n_{r_2} = 112$, respectively. The angular DOF is represented on a Legendre DVR with 235 basis functions, using symmetry restrictions and only odd rotational functions as the even ones are not allowed for O_2. The CAPs start at $7.50\,a_0$ (r_1) and $5.00\,a_0$ (r_2), with strength $0.004\,a_0^{-1}$ and order three.

The initial wavepacket Ψ_0 is represented by a Gaussian SPF in the translational DOF r_1 (with center at Q_{r_1}=$6.50\,a_0$, width $\Delta Q r_1$=$0.10\,a_0$ and initial momentum p_0 from -20 a.u. to -105 a.u.). The SPF for the bound DOF r_2 is initially set up as a vibrational eigenstate of the O_2 one-dimensional Hamiltonian, with $v = 1$ as quantum number of the initial vibrational state. The angular DOF is represented by an associated Legendre function with angular momentum of the diatomic from j=1 to j=217. The Hilbert space in the vibrational DOFs, r_1 and r_2, is spanned by 14 SPFs, while the space in the angular DOF, θ, is spanned by 10 SPFs.

To cover the entire energy range of translational energies from 0.0 eV to 5.0 eV for each selected initial state v, j, six different propagations are carried out. The resulting transition probabilities are then connected, interpolated, and smoothed to yield transition probabilities $P_{v,j}(E)$ over a fine grid supporting the desired translational energies. For very low impact energies, the transition probabilities are set to zero, since for these energies the deconvolution of translational and rovibrational contributions to the wave packet is difficult to achieve. To remedy this situation, one would need to implement an explicit adiabatic correction scheme for this system. However, for simplicity we use the related scheme already available in MCTDH [45] to address $H+H_2$ scattering so as to avoid significant recoding. Convergence in the cross sections and rates required summation over rotational momenta J from $J = 0$ to $J = 800$. Using test calculations for $J \neq 0$, we also found that the distance associated with the barrier potential is approximately $r_{1,\mathrm{barr}} = 3.8\,\text{Å}$.

III. Results

A. Transition probabilities

The calculated transition probabilities for vibrational deactivation $v = 1 \rightarrow v' = 0$, $J = 0$, and selected rotational momenta of the O_2 diatomic, j, are shown in Fig. 4. For low j ($j < 41$), the onset of the transition probabilities lies between 1–2 eV. The onset of the QCT probabilities is more abrupt than the quantum probabilities, and may be attributed to the difficulty in resolving the low-energy region accurately with QCT. In other words, the inelastic channel of rovibrational energy transfer is closed when trajectories are treated classically. Tunneling effects which may play a role in the low-energy region can only be resolved exactly by a quantum method. Both QCT and MCTDH transition probabilities level off at a value of $P(E) \approx 0.3$. This occurs at energies of 2–3 eV for low j and at energies of 0.1-1 eV for rotationally excited states. The leveling-off is explained by the contribution of alternatives channel of relaxation with $v' > v$. The rotation-vibration energy transfer takes place, since the threshold for opening of these channels depends on j. The transitions from these low-lying rotational states to the vibrational ground state are triggered by a fairly high amount of translational impact energy.

The rotational states of intermediate rotational energy, from $j = 43$ to $j = 151$, exhibit a shift of the onset of the transition probability to lower energies; also, their transition probability levels off at higher impact energies. These rotational states are still bound in the potential, and show a tendency to vibrational deactivation for low to intermediate translational energies. For high translational energies, the process of vibrational activation to the next-highest vibrational state, $v = 1 \rightarrow v' = 2$, becomes a competing process and therefore reduces the transition probability. In this region, the QCT and MCTDH transition probabilities compare very well.

For the rotational states of high rotational energy, $151 \leq j \leq 191$, the onset shifts even more to lower impact energies, and the competition with vibrational activation becomes more significant. The transition probabilities level off quickly, and QCT and MCTDH results are in good agreement, while the low-energy region is resolved better in the quantum calculations. The rotational states of highest rotational momentum, $j \geq 193$, show a similar behavior as the ones of high rotational momentum. However, in the quantum calculations, it was difficult to resolve this region accurately. We attribute this to the nature of these rotational levels: only a few of these are still bound, and the rotational levels above $j = 195$ are unbound in our MCTDH calculations. Therefore, the molecule starts to dissociate even before the impact of the Ar atom, and we chose the propagation settings (i.e., numerical grids) to represent bound wave packets. To describe this region close to the dissociation energy, we would need to extend the vibrational grid and choose a different CAP. In the QCT calculations, this energy region could be resolved without any issues.

B. Scattering cross sections

Summing over the rotational momenta J and K (MCTDH), or integrating over the impact parameter b (QCT), we can obtain the scattering cross sections for selected initial rotational states j as shown in Fig. 5. The low-lying rotational states ($j < 41$) show a steady rise of the scattering cross sections and reach about 3-4 $Å^2$, with one exception: in the quantum calculations, the lowest state j=1 reaches a scattering cross section of almost 7 $Å^2$ at 5 eV. This can be attributed to the high number of J-states that are accommodated in the averaging. Again, in the quantum method, the low-energy region is resolved better than in the QCT method because of the issues stated earlier concerning low impact energies and rotational states.

The rotational states of intermediate rotational energy, from $j = 43$ to $j = 151$, again show a shift of the onset of the cross sections as well as a decreasing cross section for higher translational energies. This effect however is mitigated compared with the transition probabilities, due to the averaging. For the very high rotational states ($j > 151$), the decrease in the cross sections due to competing processes becomes more significant. Additionally, the QCT method predicts a higher cross section than the MCTDH method for higher j; almost double for the low impact energies and $j = 181$. We attribute this deviation to the differences in the low-impact energies between QCT and MCTDH. These differences were small as the level of transition probabilities become significantly more pronounced when the averaging over the body-fixed rotational states is carried out.

The initial-state selected cross sections can be rotationally averaged over initial rotational momentum j leading to temperature-dependent cross sections such as those shown in Fig. 6. With increasing temperature, the onset of the rotationally-averaged scattering cross sections shifts to lower energies. Comparing the

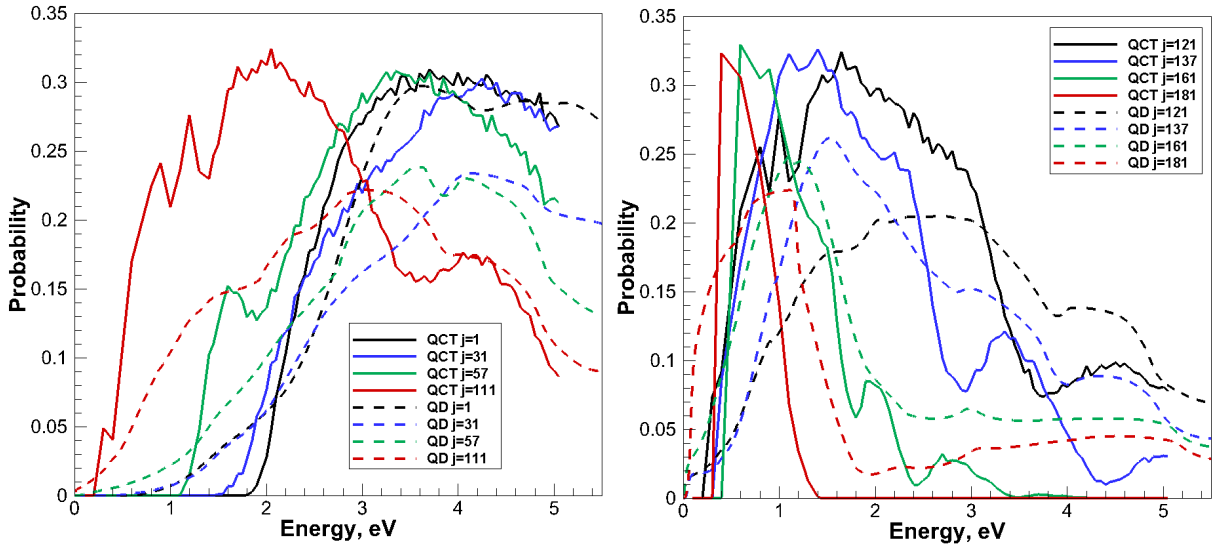

(a) j=1,31,57,111 (b) j=121,137,161,181

Fig. 4: **(A)** Final-state averaged transition probabilities obtained from MCTDH, for $v = 1 \rightarrow v = 0$, with the body-fixed and projected rotational quantum numbers $J = K = 0$ and initial j as specified. **(B)** Final-state averaged transition probabilities, QCT, for $v = 1 \rightarrow v = 0$ and initial j as specified.

quantum to the quasi-classical calculations, the quantum scattering cross sections rise slower and level off at around 3.0–3.5 Å^2. The QCT cross sections show a slightly more prominent rise and level off between 3.0–4.0 Å^2, where with higher temperature the differences between the cross sections are more pronounced than for the MCTDH results.

C. Vibration-translation rates

The rotationally-averaged scattering cross sections can be averaged over translational energies to yield rates of vibrational (de-)activation. The VT rates from the MCTDH and QCT calculations are shown in Fig. 7, for transitions $v = 1 \rightarrow v'$, $\{v' = 0, 2, 3, 5, 10, 15\}$.

The earlier onset of transition probabilities and therefore scattering cross sections in the MCTDH calculations results in a higher VT rate at lower temperatures. Also, the low-lying rotational states are resolved more accurately in the quantum method; these states dominate the low-temperature region. However, QCT and MCTDH rates agree for temperatures of 2000-3000 K and higher. At very high temperatures, the QCT rates tend to be slightly larger than the MCTDH rates. The MCTDH and QCT deactivation rates $v = 1 \rightarrow v = 0$, $v = 1 \rightarrow v = 2$ and $v = 1 \rightarrow v = 3$ show a very good agreement for higher T, while for the rates $v = 1 \rightarrow v = 5$, $v = 1 \rightarrow v = 10$ and $v = 1 \rightarrow v = 15$ the deviation between quantum and classical rates becomes larger also at high temperatures. Generally, the differences between MCTDH and QCT scattering cross sections are less pronounced than the differences in the transition probabilities due to the strongly averaging procedure that converts molecular trajectory information into macroscopic quantities.

D. Vibrational relaxation times

The VT rates cannot be measured directly in the experiment, the only way to compare the calculated data to the experiment is via the vibrational relaxation times. However, this involves a conversion of the experimentally measured data into relaxation times, as well as a conversion of the theoretical data; this introduces some uncertainties in the comparison, as it involves inherent assumptions such as the adsorption coefficient being independent of the rotational state, and vibrational harmonicity. Nevertheless, the experimental measurements give insights into the accuracy of the theoretical calculation, and the applicability of the quantum and quasi-classical methods. In the present studies, two experimental data sets are used to assess the adopted computational models. The vibrational relaxation times in O_2–Ar collisions were reported

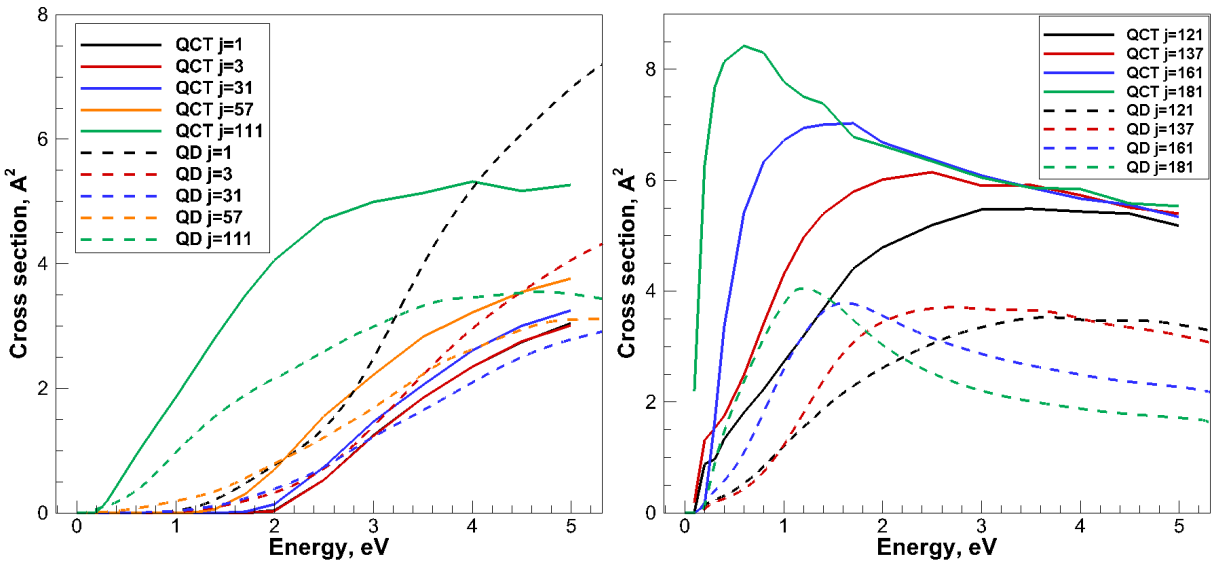

(a) j=1,3,31,57,111 (b) j=121,137,161,181

Fig. 5: **(A)** Scattering cross sections as calculated with MCTDH, for $v = 1 \rightarrow v = 0$ and initial j as specified. **(B)** Scattering cross sections calculated with the QCT method, for $v = 1 \rightarrow v = 0$ and initial j as specified.

for the first time by Camac, [7] where the ultraviolet absorption technique was applied to collect data in O_2–Ar mixtures with the post-shock translational temperatures between 1200 and 8000 K. The absorption in Schumann-Runge bands was measured at 147 nm wavelength. Recently, the O_2–Ar molecular system was revisited by Hanson and co-workers [8] using similar methods of laser abortion spectroscopy in the range between 1000 and 4000 K. For this purpose, a picosecond pulsed Ti:Sapphire laser was used to generate tunable UV light with the wavelength between 210 and 230 nm. The new data has much less scatter compared to the earlier measurements by Camac.

The calculated and experimental vibrational relaxation times are shown in Fig. 8. The present theoretical data is constructed from two different equations, Eq. (29) and Eq. (30), and for QCT also from the solution of the system of master equations. The MCTDH data is shown with black curves, while the QCT results are shown in red. The curve attributed to Millikan and White is obtained from their empirical model using the specific parameters for the O_2–Ar system [41]. Symbols represent the experimental data from Ref. [7], for different admixtures of O_2 in Ar, and from Ref. [8].

The experimental and empirical relaxation times are in excellent agreement which is not surprising since the Millikan-White model is based on the experimental data from Ref. [7]. The data by Camac is confirmed by the recent experimental measurements by the Hanson group [8]. The relaxation time derived from MCTDH calculations using Eq. (30) is in good agreement with the experimental data. There is a slight underestimation of experimental data by the MCTDH method at temperatures between 1000 and 4000 K. It will be shown later that the implementation of a more repulsive PES leads to an increase of $p\tau_{vib}$ at low temperatures without effecting the relaxation time at high temperature limit. Taking this into account, a better agreement between MCTDH calculations and the experimental data can be expected using more accurate PES.

The QCT method strongly overestimates the vibrational relaxation time at temperatures below 4000 K. This is in agreement with the results shown in Fig. 7: the QCT VT rates are generally smaller than the MCTDH rates. This is due to the insufficient statistics accumulated by the QCT method. Because the true O_2–Ar vibrational relaxation time increases by orders of magnitude in the low temperature region, the QCT method requires a proportional increase of the number of trajectories in each batch. This makes the QCT calculations impractical for the system of interest at low translational temperatures. Recently, a similar failure of the quasi-classical methods regarding the O_2–N_2 system was described in Ref. [46]. Notably, once the translational temperature is high enough to accumulate the statistics using a reasonable amount of

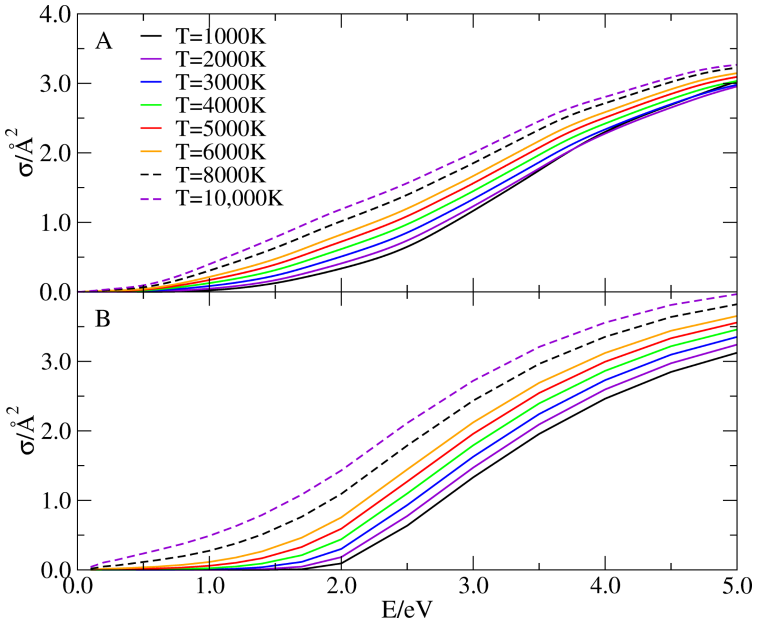

Fig. 6: **(A)** Rotationally averaged scattering cross sections as calculated with MCTDH, for $v = 1 \rightarrow v = 0$ and rotational temperature T as specified. **(B)** Rotationally averaged scattering cross sections as calculated wit the QCT method, for $v = 1 \rightarrow v = 0$ and rotational temperature T as specified.

trajectories, the QCT and MCTDH methods demonstrate a very good agreement.

In our dynamics treatment, we only involve the O_2 electronic ground state. The other low-lying electronic states of O_2 also become accessible at the high temperatures discussed here, and part of the deviation between theory and experiment may also result from the neglect of nonadiabatic couplings at high temperatures.

In addition to nonadiabatic couplings, failures in the assumption that the system is in an equilibrium state (in the sense that Boltzmann distributions are satisfied for translational, rotational and vibrational degrees of freedom at the same temperature), may also lead to a further deviation between theoretical and experimental results. To confirm this origin of the deviation, details of the state distributions of the system as well as the related temperatures would need to be experimentally available. Using such data, we would be able to generate nonequilibrium rates and lifetimes, and could investigate the impact of the nonequilibrium effects on the accuracy of the calculation. This will be a future point for studies, and can easily be implemented in our VT rate and lifetime calculations.

Finally, the approximation that J–K coupling can be ignored (i.e. centrifugal sudden (CS) approximation), could introduce uncertainties in the quantum dynamics simulations. On another system, the H_2 + D_2 scattering system, J-K coupling has been shown to enhance the reactivity [47]. In line with this finding, a more accurate kinetic energy operator in which J–K coupling is treated accurately, could lead to slightly enhanced transition probabilities and therefore higher VT rates (lower relaxation time). At this point, we chose to neglect J–K coupling due to the additional computational demand it introduces in the calculation, and since we also do not treat the J–K dependence of the transition probabilities explicitly.

In summary, the use of Eq. (29) leads to underestimates in relaxation times, especially at high temperatures. This is due to the influence of the reverse excitation process. It affects both QCT and MCTDH methodologies. At low temperatures, the excitation events are rare; relaxation times via Eqs. (29) and (30) are nearly identical. The QCT master equation relaxation time lies in between the two approaches. This more accurate approach at calculating relaxation times takes into account multiquantum transitions, and was only carried out for the QCT rates, since the full set of $v = x \rightarrow v = y$, $\{x, y = 0, 1, \ldots, 36\}$ transition rates are required. At this point, we only generated quantum-mechanical rates involving the first vibrational excited state.

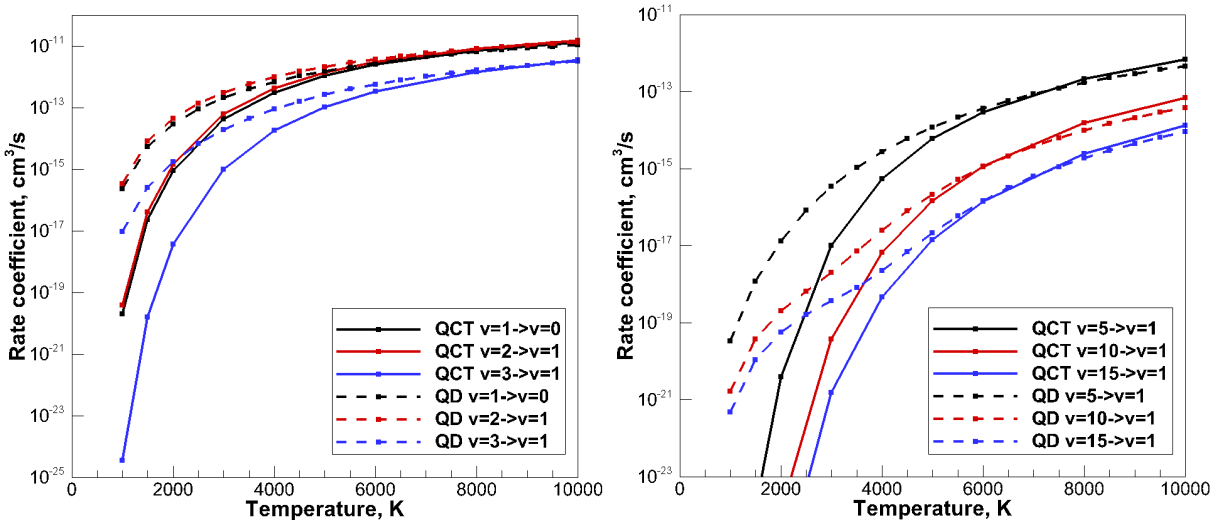

(a) v'=1,2,3; v=0,1 (b) v'=5,10,15, v=1

Fig. 7: Vibration-translation rates from MCTDH and QCT calculations, for vibrational deactivation from $v' \to v$.

E. Effect of impact angle on relaxation

Due to difficulties arising from the evaluation of the CCSD potential in the vicinity of O_2 right turning points, the present work does not provide a global curve fit of the CCSD potential, and its implementation in the QCT method coupled with the multi-reference PES calculations is left for the future. However, taking into account that the CCSD potential retains the exponential shape of the repulsive wall which is less steep than that of the analytical potential, a parametric study of vibrational relaxation time using the QCT method is conducted. In these simulations, the variation of the repulsive parameter B (Table 1) is adopted. In addition to the recommended value of 3.8 Å, B is set to 3.2 and 3.5 Å. All other parameters are kept the same. The variation of vibrational relaxation time with B is shown in Fig. 9.

The vibrational relaxation times increases at a smaller value of B, as follows from the relaxation time derived from the rate of monoquantum deactivation from $v = 1$. This effect is most pronounced at low temperatures while changes of $p\tau_v$ at T >8000 K are quite small. Taking into account that the QCT method tends to overestimate the relaxation time at low temperatures, as follows from Fig. 8, the implementation of more accurate PES will increase the QCT vibrational relaxation time. Thus, the influence of the quantum effects on QCT results will be even more pronounced on *ab-initio* PES. Again, the accurate estimation of quantum effects would include the multi-reference characterization of O_2–Ar electronic wave function.

The probability of vibrational deactivation at different impact angles is shown in Fig. 10. These calculations are performed for the initial state of oxygen with $v = 1$, $j = 0$. The head-on collision at zero degrees does not necessary lead to faster vibrational deactivation compared to collisions at non-zero angle between O–O and O_2–Ar. In fact, the channel of vibrational deactivation opens at smaller energies at the intermediate value of impact angle, i.e. at 40 degrees. These results demonstrate that a more accurate simulation of vibrational energy transfer in O_2–Ar collisions would involve an evaluation of an *ab-initio* potential in the entire range of impact angles.

A different situation takes place when the dependence of rotational relaxation on the impact angle is studied. The probability of transition from $(v = 1, j = 0)$ to $(v = 1, j \neq 0)$ is shown in Figs. 11a and 11b at collisional energies of 1 and 3 eV. For vibrationally elastic transitions with the change of rotational quantum number, a strong dependence on the impact angle is observed. A head-on collisions are efficient for rotational excitation of molecule with the probability increasing toward to nearly rotationally inelastic collisions as well as to the collisions with the large rotational jump. For collisions at non-zero impact angle, states with high rotational numbers are not accessible. At 80 degrees of impact angle transitions to only neighboring rotational states occur. At higher kinetic energies the range of accessible rotational states becomes wider

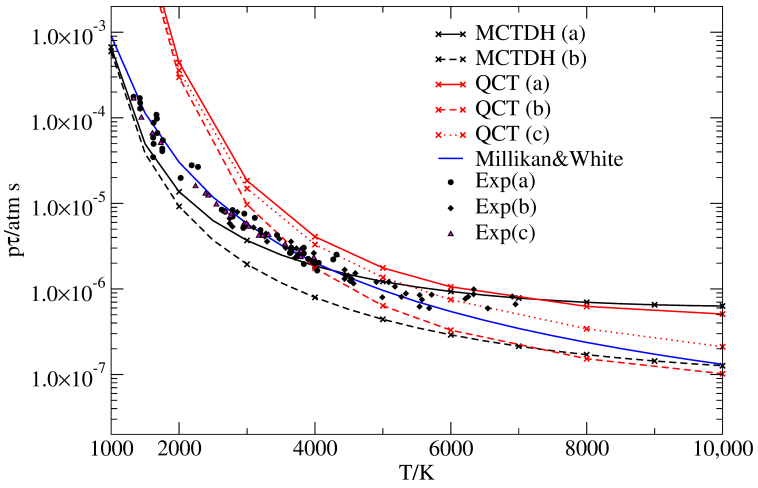

Fig. 8: Vibrational relaxation times, experiment data and MCTDH and QCT methods. The theoretical relaxation times are obtained using different approximations (MCTDH (a) and QCT (a) using Eq. (29), MCTDH (b) and QCT (b) using Eq. (30), and QCT (c) using master equation calculations). The Millikan-White data is generated according to the empirical model in Ref. [41]. The experimental data included was obtained for different gas mixtures (Exp(a): 0.25% O_2 and 99.75% Ar, and 1.0%O_2 and 99.0% Ar (Ref. [7]); Exp(b): 21.5% O_2 and 78.5% Ar (Ref. [7]); Exp(c): 1.0% O_2 and 99.0% Ar (Ref. [8]).

but the overall behavior remains similar to that at 1 eV.

IV. Discussion and Conclusion

The transition probabilities and scattering cross sections calculated with the MCTDH and QCT methods compare quite well, especially for moderate to high translational energies. The O_2–Ar scattering for high initial rotational states are better resolved with the classical method, while the low-lying rotational states and low impact energies are more accurately obtained using MCTDH. After averaging the cross sections over impact energies to generate rates of vibrational deactivation, we found that quantum-mechanical and classical rates agree quite well above 3000 K. Below that temperature range, the QCT method fails to predict the rates accurately, as can be expected from a quasi-classical method that does not completely account for tunneling and other quantum effects. The MCTDH method tends to slightly underestimate the vibrational relaxation time in the range between 1000 and 4000 K. This may be attributed to the fact that the analytical PES is more repulsive than the *ab-initio* PES generated by the CCSD calculations. Tor the remaining temperature range, from 4000-10,000 K, both sets of rates show very good agreement.

The standard procedure for obtaining fully quantum-mechanical and quasi-classical VT rate calculations is determined. In this approach, we make use of the capture model to generate transition probabilities for rotationally excited states in the body-fixed frame. Both the MCTDH and QCT methods have significant computational requirements. For the quantum-mechanical calculations, six propagations per O_2 rovibrational state were carried out to cover the entire range of impact energies. Each propagation takes about six hours on average on a single core on the Stampede cluster at Texas Advance Supercomputing Center, yielding to 36 h of computation for each rovibrational state. In total, for initial vibrational state $v = 1$ and all 217 initial rotational states, the quantum-mechanical calculations took about 7800 h computing time on a single node. The QCT calculations for $v = 1$ and all possible j require 790 h with the fixed size of a batch equal to 2000 trajectories. Hence, each rovibrational state takes approximately 4 h to obtain the data in the entire range of collision energies. The computational time is directly proportional to the size of a batch. Trajectory propagation for excited pre-collisional vibrational states require higher computational time due to increased impact parameter b_{max}. Overall, the MCTDH approach appears to be an order of magnitude more expensive than the QCT calculations. However, in light of the much better resolution of the vibrational relaxation times at low temperatures, the MCTDH method is recommended over the QCT approach for conditions when vibrational deactivation events are rare.

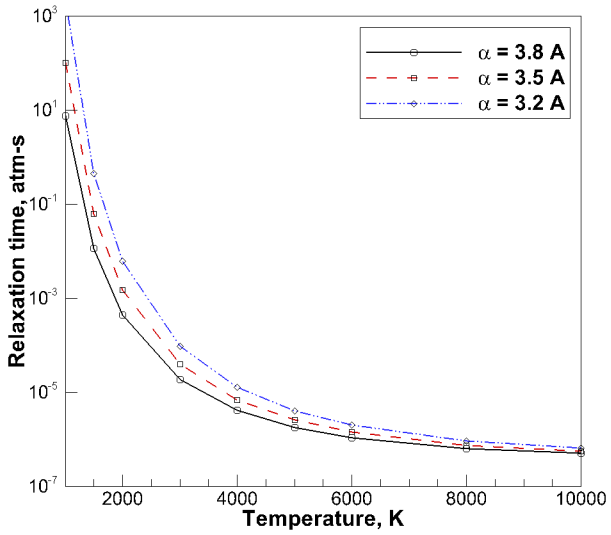

Fig. 9: QCT vibrational relaxation time obtained at different values of the repulsive O_2–Ar parameter

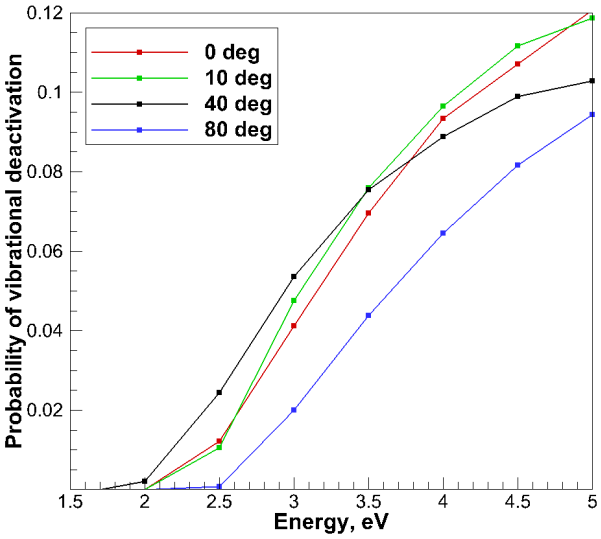

Fig. 10: Variation of transition probability of vibrational deactivation with the impact angle

The quantum-mechanical VT rates for transitions $v = 1 \rightarrow v' = \{0, 2, 3, \ldots, 15\}$ and the QCT VT rates for all the possible initial rovibrational states in the temperature range from 1000 K to 10,000 K are available upon request. The inclusion of excited vibrational states and corresponding single- and multi-state quantum transitions is important for constructing reliable models of thermodynamics at temperatures relevant to hypersonic flows. Despite the fact that the quantum-mechanical simulations in the present work are limited to $v = 1$, the MCTDH approach seems to be a valuable tool for resolving the collisional dynamics of the entire rovibrational ensemble.

An influence of the impact angle on vibrational and rotational relaxation is studied. For nearly all values of impact angle, the ab-initio CCSD PES appears to be less repulsive than the analytical PES. The vibrational deactivation from the first excited state is equally probable for all values of impact angles. Finally, the probability of rotational transition in vibrationally elastic collisions strongly depends on the impact angle. At impact angles close to $\pi/2$ the probability of rotational transition drops significantly.

Using our models, we obtain very good agreement of calculated, experimental and empirical data over the entire temperature range. It is now possible to improve the data obtained by the QCT method so as to bridge the gap between low (1000 K) and high (10,000 K) temperatures, yielding to very accurate data for future aerodynamics simulations.

Acknowledgments

I. U. and R. H. thank Hans-Dieter Meyer for helpful discussions and for providing the MCTDH package. This work has been partially supported by the Air Force Office of Scientific Research through Grant No. FA9550-16-1-0291. I. U. acknowledges the Alexander von Humboldt Foundation, Germany, for support through a Feodor Lynen Fellowship. This work used HPC resources (Stampede) at the Texas Advanced Computing Center (TACC) at the University of Texas at Austin through an XSEDE allocation under award No. TG-CTS090079.

References

[1]Vincenti, W. G. and Charles H. Kruger, J., *Introduction to physical gas dynamics*, Robert E. Krieger Publishing Company, Huntington, New York, reprint 1977 ed., 1967.

[2]Park, C., *Nonequilibrium hypersonic aerothermodynamics*, Wiley, New York, 1989.

[3]Kim, J. G. and Boyd, I. D., "State-resolved master equation analysis of thermochemical nonequilibrium of nitrogen," *Chem. Phys.*, Vol. 415, 2013, pp. 237–246.

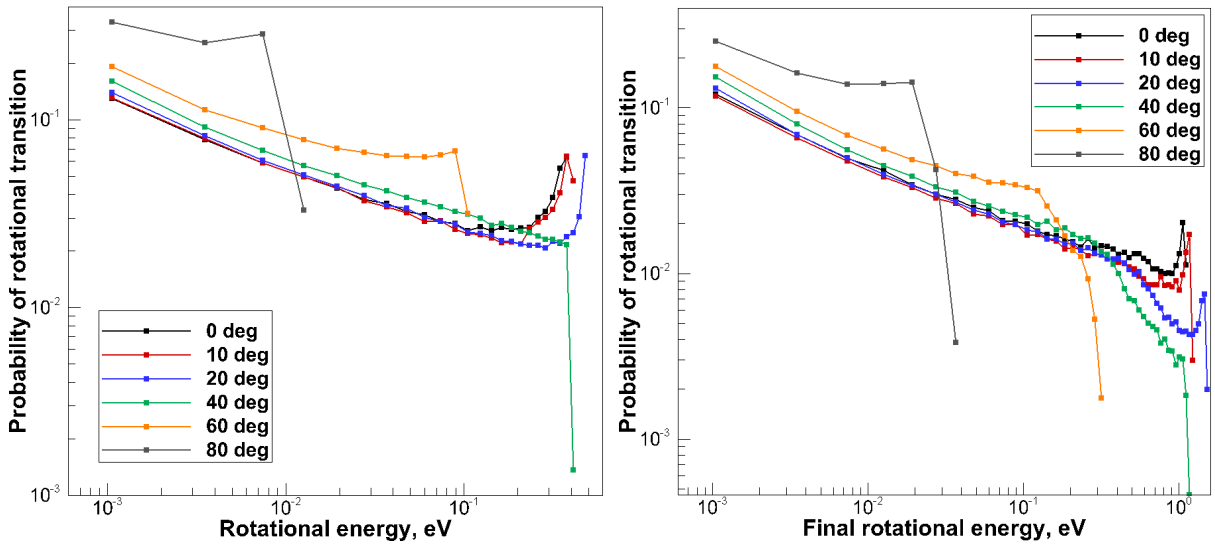

(a) Collisional energy of 1eV

(b) Collisional energy of 3eV

Fig. 11: Variation of probability of rotational transition with the impact angle

[4]Esposito, F. and Capitelli, M., "Quasiclassical trajectory calculations of vibrationally specific dissociation cross-sections and rate constants for the reaction O + O_2 = 3O," *Chem. Phys. Lett.*, Vol. 364, 2002, pp. 180–187.

[5]Andrienko, D. A. and Boyd, I. D., "High fidelity modeling of thermal relaxation and dissociation of oxygen," *Phys. Fluids*, Vol. 27, No. 11, 2015, pp. 116101.

[6]Capitelli, M., Ferreira, C. M., Gordiets, B. F., and Osipov, A. I., *Plasma kinetics in atmospheric gases*, Vol. 31, Springer Science & Business Media, 2013.

[7]Camac, M., "O_2 Vibration Relaxation in Oxygen-Argon Mixtures," *J. Chem. Phys.*, Vol. 34, 1961, pp. 448–459.

[8]Owen, K. G., Davidson, D. F., and Hanson, R. K., "Oxygen Vibrational Relaxation Times: Shock Tube/Laser Absorption Measurements," *Journal of Thermophysics and Heat Transfer*, 2015, pp. 1–8.

[9]Meyer, H.-D., Manthe, U., and Cederbaum, L. S., "The multi-configurational time-dependent Hartree approach," *Chem. Phys. Lett.*, Vol. 165, 1990, pp. 73–78.

[10]Meyer, H.-D., "Studying molecular quantum dynamics with the multiconfiguration time-dependent Hartree method," *WIREs: Comput. Mol. Sci.*, Vol. 2, 2012, pp. 351–374.

[11]Meyer, H.-D., Gatti, F., and Worth, G. A., editors, *Multidimensional Quantum Dynamics: MCTDH Theory and Applications*, Wiley-VCH, Weinheim, 2009.

[12]Esposito, F., Armenise, I., and Capitelli, M., "N-N_2 state to state vibrational-relaxation and dissociation rates based on quasiclassical calculations," *Chem. Phys.*, Vol. 331, 2006, pp. 1–8.

[13]Andrienko, D. and Boyd, I. D., "Investigation of oxygen vibrational relaxation by quasi-classical trajectory method," *Chem. Phys.*, Vol. 459, 2015, pp. 1–13.

[14]Everitt, K. F. and Skinner, J. L., "Vibrational energy relaxation of oxygen in liquid mixtures with argon," *J. Chem. Phys.*, Vol. 110, 1999, pp. 4467–4470.

[15]Tong, X., Nagy, T., Reyes, J. Y., Germann, M., Meuwly, M., and Willitsch, S., "State-selected ionmolecule reactions with Coulomb-crystallized molecular ions in traps," *Chem. Phys. Lett.*, Vol. 547, 2012, pp. 1–8.

[16]Steele, D. and Lippincott, E. R., "Comparative study of empirical internuclear potential functions," *Rev. Mod. Phys.*, Vol. 34, 1962, pp. 239–251.

[17]Vanderslice, J. T., Mason, E. A., Maisch, W. G., and Lippincott, E. R., "Ground state of hydrogen by the Rydberg-Klein-Rees method," *J. Molec. Spectrosc.*, Vol. 3, 1959, pp. 17–29.

[18]Kim, J. G. and Boyd, I. D., "Thermochemical nonequilibrium modeling of electronically excited molecular oxygen," *11th AIAA Aviation/ASME Joint Thermophysics and Heat Transfer Conference*, 2014.

[19]Gross, A. and Billing, G. D., "Rate constants for ozone formation," *Chem. Phys.*, Vol. 187, 1994, pp. 329–335.

[20]Kroes, G. J. and Rettschnick, R. P. H., "Vibrational relaxation of glyoxal in collisions with He and Ar," *Chem. Phys.*, Vol. 156, 1991, pp. 293–307.

[21]Gross, A. and Billing, G. D., "Rate constants for ozone formation," *Chem. Phys.*, Vol. 187, No. 3, 1994, pp. 329–335.

[22]Mizobata, K., "An analysis of quasiclassical molecular collisions and rate processes for coupled vibration-dissociation and recombination," *AIAA*, 1997, pp. 97–0132.

[23]Varandas, A. J. C., "Four-atom bimolecular reactions with relevance in environmental chemistry: Theoretical work," *Int. Rev. Phys. Chem.*, Vol. 19, No. 2, 2000, pp. 199–245.

[24]Irikura, K. K., "Experimental Vibrational Zero-Point Energies: Diatomic Molecules," *J. Phys. Chem. Ref. Data*, Vol. 36, 2007, pp. 389–397.

[25]Huber, K. P. and Herzberg, G., *Molecular Spectra and Molecular Structure. IV. Constants of Diatomic Molecules*, Van Nostrand Reinhold Co., 1979.

[26]Beck, M. H., Jäckle, A., Worth, G. A., and Meyer, H.-D., "The multiconfiguration time-dependent Hartree (MCTDH) method: A highly efficient algorithm for propagating wavepackets," *Phys. Rep.*, Vol. 324, 2000, pp. 1–105.

[27]Schmidt, M. W., Baldridge, K. K., Boatz, J. A., Elbert, S. T., Gordon, M. S., Jensen, J. H., Koseki, S., Matsunaga, N., Nguyen, K. A., Su, S., Windus, T. L., Dupuis, M., and Montgomery, J. A., "General Atomic and Molecular Electronic Structure System," *J. Comput. Chem.*, Vol. 14, 1993, pp. 1347–1363.

[28]Bentz, J. L., Olson, R. M., Gordon, M. S., Schmidt, M. W., and Kendall, R. A., *Comput. Phys. Commun.*, Vol. 176, 2007, pp. 589–600.

[29]Francl, M. M., Pietro, W. J., Hehre, W. J., Binkley, J. S., Gordon, M. S., DeFrees, D. J., and Pople, J. A., *J. Chem. Phys.*, Vol. 77, 1983, pp. 3654–3665.

[30]Bytautas, L. and Ruedenberg, K., "Accurate ab initio potential energy curve of O2. I. Nonrelativistic full configuration interaction valence correlation by the correlation energy extrapolation by intrinsic scaling method," *Journal of Chemical Physics*, Vol. 132, No. 7, 2010.

[31]Bytautas, L., Matsunaga, N., and Ruedenberg, K., "Accurate ab initio potential energy curve of O2. II. Core-valence correlations, relativistic contributions, and vibration-rotation spectrum," *Journal of Chemical Physics*, Vol. 132, No. 7, 2010.

[32]Adamovich, I. V. and Rich, J. W., "Three-dimensional nonperturbative analytic model of vibrational energy transfer in atom–molecule collisions," *Journal of Chemical Physics*, Vol. 109, No. 18, 1998, pp. 7711–7724.

[33]Jäckle, A. and Meyer, H.-D., "Product representation of potential energy surfaces," *J. Chem. Phys.*, Vol. 104, 1996, pp. 7974.

[34]Riss, U. V. and Meyer, H.-D., "Calculation of resonance energies and widths using the complex absorbing potential method," *J. Phys. B*, Vol. 26, 1993, pp. 4503.

[35]Riss, U. V. and Meyer, H.-D., "Investigation on the reflection and transmission properties of complex absorbing potentials," *J. Chem. Phys.*, Vol. 105, 1996, pp. 1409.

[36]Tannor, D. J. and Weeks, D. E., "Wave packet correlation function formulation of scattering theory: The quantum analog of classical S-matrix theory," *J. Chem. Phys.*, Vol. 98, 1993, pp. 3884–3893.

[37]Bulut, N., Castillo, J. F., Aoiz, F. J., and nares, L. B., "Real wave packet and quasiclassical trajectory studies of the H^+ + LiH reaction," *Phys. Chem. Chem. Phys.*, Vol. 10, 2008, pp. 821–827.

[38]Sun, Q., Bowman, J. M., Schatz, G. C., Sharp, J. R., and Connor, J. N. L., "Reduced-dimensionality quantum calculations of the thermal rate coefficient for the Cl+HCl →ClH+Cl reaction: Comparison with centrifugal-sudden distorted wave, coupled channel hyperspherical, and experimental results," *J. Chem. Phys.*, Vol. 92, 1990, pp. 1677–1686.

[39]Gray, S. K., Goldfield, E. M., Schatz, G. C., and Balint-Kurti, G. G., "Helicity decoupled quantum dynamics and capture model cross sections and rate constants for $O(^1D) + H_2 \rightarrow OH + H$," *Phys. Chem. Chem. Phys.*, Vol. 1, 1999, pp. 1141–1148.

[40]Truhlar, D. G. and Muckerman, J. T., "Reactive scattering cross sections III: quasiclassical and semiclassical methods," *Atom-Molecule Collision Theory*, Springer, 1979, pp. 505–566.

[41]Millikan, R. C. and White, D. R., "Systematics of Vibrational Relaxation," *J. Chem. Phys.*, Vol. 39, 1963, pp. 3209–3213.

[42]Panesi, M., Jaffe, R. L., Schwenke, D. W., and Magin, T. E., "Rovibrational internal energy transfer and dissociation of $N_2(^1\Sigma_g^+)$- $N(^4S_u)$ system in hypersonic flows," *J. Chem. Phys.*, Vol. 138, No. 4, 2013, pp. 044312.

[43]Andrienko, D. A. and Boyd, I. D., "High Fidelity Modeling of Thermal Relaxation and Dissociation of Oxygen," 45th AIAA Thermophysics Conference, AIAA Paper 2016-0736, January 2016.

[44]Park, C., "Rotational relaxation of N_2 behind a strong shock wave," *J. Thermophys. Heat Tr.*, Vol. 18, No. 4, 2004, pp. 527–533.

[45]Worth, G. A., Beck, M. H., Jäckle, A., and Meyer, H.-D., The MCTDH Package, Version 8.2, (2000). H.-D. Meyer, Version 8.3 (2002), Version 8.4 (2007). Current version: 8.4.11 (2015). See http://mctdh.uni-hd.de/.

[46]Garcia, E., Kurnosov, A., Lagana, A., Pirani, F., Bartolomei, M., and Cacciatore, M., "Efficiency of Collisional O_2+ N_2 Vibrational Energy Exchange," *J. Phys. Chem. B*, 2015.

[47]Sukiasyan, S. and Meyer, H.-D., "On the Effect of Initial Rotation on Reactivity. A Multi-Configuration Time-Dependent Hartree (MCTDH) Wave Packet Propagation Study on the H + D_2 and D + H_2 Reactive Scattering Systems," *J. Phys. Chem. A*, Vol. 105, 2001, pp. 351–374.